Classical-Quantum Correspondence for Above-Threshold Ionization

Min Li,[1] Ji-Wei Geng,[1] Hong Liu,[1] Yongkai Deng,[1] Chengyin Wu,[1,2] Liang-You Peng,[1,2] Qihuang Gong,[1,2,*] and Yunquan Liu[1,2,†]

[1]*State Key Laboratory for Mesoscopic Physics and Department of Physics, Peking University, Beijing 100871, People's Republic of China*

[2]*Collaborative Innovation Center of Quantum Matter, Beijing 100871, China*

(Received 6 November 2013; published 17 March 2014)

We measure high resolution photoelectron angular distributions (PADs) for above-threshold ionization of xenon atoms in infrared laser fields. Based on the Ammosov-Delone-Krainov theory, we develop an intuitive quantum-trajectory Monte Carlo model encoded with Feynman's path-integral approach, in which the Coulomb effect on electron trajectories and interference patterns are fully considered. We achieve a good agreement with the measured PADs of atoms for above-threshold ionization. The quantum-trajectory Monte Carlo theory sheds light on the role of ionic potential on PADs along the longitudinal and transverse direction with respect to the laser polarization, allowing us to unravel the classical coordinates (i.e., tunneling phase and initial momentum) at the tunnel exit for all of the photoelectrons of the PADs. We study the classical-quantum correspondence and build a bridge between the above-threshold ionization and the tunneling theory.

DOI: 10.1103/PhysRevLett.112.113002 PACS numbers: 32.80.Rm, 31.90.+s, 32.80.Fb, 32.80.Wr

As a benchmark experiment, the observation of above-threshold ionization (ATI) has significantly motivated the progress of strong-field physics [1]. ATI can be usually understood within the scenario of multiphoton absorption through resonant states (so-called Freeman resonance [2]) or nonresonant states. Alternatively, increasing the laser intensity, the potential barrier of an atom is suppressed drastically and electrons can easily tunnel out. Usually, multiphoton ionization and tunneling ionization are distinguished by the Keldysh parameter γ [3] [$\gamma = \sqrt{I_p/2U_p}$, where I_p is the ionization potential, U_p the ponderomotive potential ($U_p = E_0^2/4\omega^2$), E_0 the field amplitude, ω the field frequency, and atomic units are used throughout unless otherwise specified]. Tunneling ionization will dominate if $\gamma < 1$, while multiphoton ionization prevails when $\gamma > 1$. A thorough understanding of atomic ionization in strong fields is essential for further explorations and diverse applications.

The intuitive understanding of strong-field ionization arises mainly from Simpleman's picture [4], in which the tunneled electrons oscillate classically in the laser field after ionization. This model, although successful in providing many useful qualitative predictions, has not been able to provide a quantitative fit with the experimental data due to the shortcoming in handling the Coulomb potential of the parent ion and quantum effect. Usually, the ionic potential is ignored in the framework of the strong-field approximation (for a review, see [5]). Recently, the classical-trajectory Monte Carlo simulation (CTMC) [6] and Coulomb-corrected strong-field approximation [7,8] models can provide more quantitative description of strong-field ionization. More accurately, one can reproduce the resonant features present in ATI spectra with astonishing precision by solving the time-dependent Schrödinger equation for model atomic potentials [9]. However, because the quantum simulation is not physically transparent, no simple picture can be drawn for the mechanism leading to ATI.

Strong-field ionization is also usually described with the Ammosov-Delone-Krainov (ADK) theory, in which the ionization rate, the tunnel exit, and the momentum distribution are prescribed [10,11]. In this Letter, we develop an intuitive quantum-trajectory Monte Carlo (QTMC) model for strong-field ionization combining the ADK theory with Feynman's path-integral approach [12]. The use of path integrals for quantizing classically mechanical systems can be traced back to Dirac's idea [13,14]. The path-integral approach has been employed for intense-laser-atom interaction [15], where the Coulomb potential was completely ignored. Our QTMC model fully includes both the Coulomb potential and quantum interference effect after the tunneling. The QTMC model further allows us to reproduce the photoelectron angular distributions (PADs) of ATI and to achieve deep understanding of the experimental results in terms of classical trajectories of the tunneled electrons in conjunction with the "quantum" treatment. We show that the Coulomb potential manifests its importance in both the trajectory and phase of the tunneled electrons, which has a significant effect on PADs along both the longitudinal and transverse directions with respect to the laser polarization.

Experimentally, using cold-target recoil-ion reaction momentum spectroscopy (COLTRIMS) [16], we have measured two-dimensional PADs of multiphoton ionization of rare gases by a Ti:sapphire laser. The typical measured

PAD of Xe is shown in Fig. 1(b) at the intensity of 0.75×10^{14} W/cm^2 (795 nm, 25 fs), which is dominated by a series of concentric rings centered at zero, corresponding to the characteristic ATI peaks.

To shed a direct light on the PAD of ATI, we perform the calculations with the QTMC model. Briefly, we sample the initial coordinates of all of the tunneled electrons at the tunnel exit using the ADK theory. The tunnel exit is derived from the Laudau's effective potential theory [17]. As illustrated in Fig. 1(a), after tunneling, the electron motion in the combined laser and Coulomb fields is governed by the Newtonian equations, $\ddot{\mathbf{r}} = -\mathbf{r}/r^3 - \mathbf{E}(t)$, where r is the distance between electron and nucleus. In the QTMC model, we have included the phase for each electron with e^{-iS} (S is the classical action after tunneling). Including the Coulomb effect, the classical action after the tunnel exit is given by $S = \int_{t_0}^{\infty}[\mathbf{v}(t)^2/2 - 1/|\mathbf{r}(t)| + I_p]dt$, where t_0 is the instant of tunneling, $\mathbf{v}(t)$ is the electron velocity, and I_p is the ionization potential. The phase is contributed by three terms, i.e., the trajectory phase related with the motion in the laser field $\Phi^L = \int_{t_0}^{\infty}\mathbf{v}(t)^2/2dt$, the constant phase related with the ionization potential$\Phi^I = \int_{t_0}^{\infty} I_p dt$, and the Coulomb-corrected phase $\Phi^C = \int_{t_0}^{\infty} -1/|\mathbf{r}(t)|dt$. Note that the classical action S is integrated with time together with the Newtonian equations, and thus the Coulomb effect is fully considered in the QTMC model. The comparison of the Simpleman, CTMC, and QTMC models is described in [18].

The simulated two-dimensional PAD of multiphoton ionization from Xe at 0.75×10^{14} W/cm^2 [Fig. 1(d)] agrees well with the experiment. We further show the calculated PADs of Xe at 0.5×10^{14} W/cm^2 in Fig. 1(c).

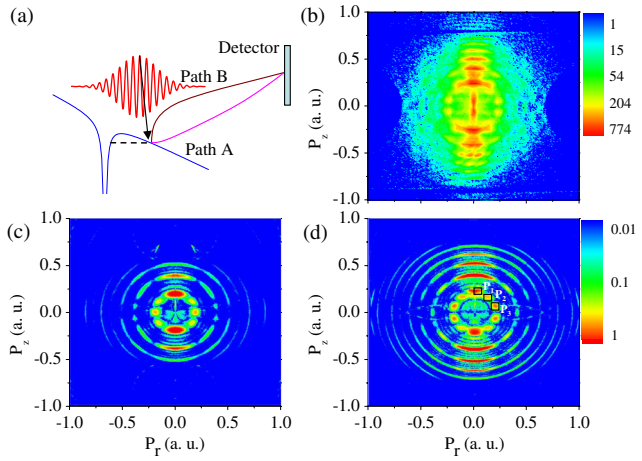

FIG. 1 (color online). (a) Illustration of the QTMC model. After the tunneling, electrons could follow different paths, i.e., path A and path B, have the same final momenta on the detector, and will interfere with each other. (b) The experimental PAD of Xe at 0.75×10^{14} W/cm^2. (c) and (d) show the simulated PADs of Xe at 0.5×10^{14} and 0.75×10^{14} W/cm^2, respectively. Note that the focus volume effect is not considered in the calculation.

One can find that the dominant angular momentum of the first-order ATI is $L = 4$. At 0.75×10^{14} W/cm^2, the dominant angular momentum of the first-order ATI is $L = 5$. The multiphoton channel-switching effect can be reproduced [19,20].

The Coulomb potential is very important in the strong-field atomic ionization. However, this effect cannot be directly unraveled by the quantum simulation. As seen in the QTMC model, the Coulomb effect plays essential roles in the two aspects: (i) the electron motion in the Newtonian equations and (ii) the phase and trajectory in the phase equation. We can separate the Coulomb effect in both the Newtonian and phase equations using the QTMC model. We first show the calculated PAD within the Simpleman model in Fig. 2(a). Compared to the PAD calculated by the CTMC model in Fig. 2(b), it is distorted by the strong scattering in the presence of the Coulomb potential. However, the results of both the Simpleman and CTMC models deviate very much from the experimental measurement if the interference effect is not included.

When the Coulomb effect is not included in both the Newtonian equations and the phase equation after tunneling in the QTMC model, the characteristic ATI rings will appear [Fig. 2(c)]. The simulated PAD by the QTMC model

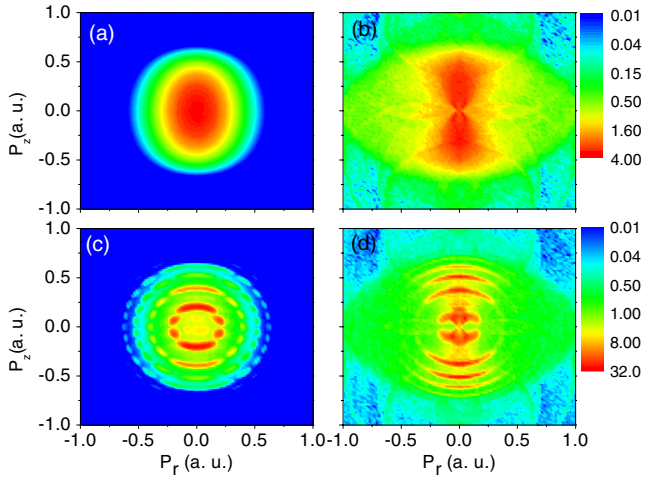

FIG. 2 (color online). (a) The simulated PAD of Xe without the Coulomb potential in the Newtonian equation and without solving the phase equation. (b) The simulated PAD of Xe with the Coulomb effect in the Newtonian equation but without solving the phase equation (CTMC model). (c) The simulated PAD of Xe without consideration of the Coulomb effect in both the Newtonian equation and phase equation. (d) The simulated PAD of Xe with the Coulomb effect in the Newtonian equation and without the Coulomb-corrected phase. Only the Newtonian equations are solved in (a) (without the Coulomb potential) and (b) (with the Coulomb potential). The Newtonian and phase equations are solved simultaneously in (c) and (d). In (c), the Coulomb potential is not considered in both equations. In (d), the Coulomb potential is considered in both equations, but without the term of the Coulomb-corrected phase.

reveals the so-called "interference carpet" structure [21]. When the Coulomb potential is fully included, the relative contribution of each ATI spot is redistributed and most of events are shifted along the laser polarization direction because of the Coulomb focusing effect [22], as seen in Fig. 1(d). In order to achieve deep understanding on the Coulomb effect on the PAD of ATI, we also calculated the PADs with the inclusion of the Coulomb effect in the Newtonian equations, but not included for the phase equation in the QTMC model. As illustrated in Fig. 2(d), interestingly, without the Coulomb-corrected phase in the action, one can only observe the ATI along the longitudinal direction (parallel to the laser polarization). This indicates that the Coulomb-corrected phase plays an essential role in the formation of ATI spots transverse to the laser polarization, i.e., the interference carpet. To shed more light on that, we must study the tunneling coordinates of ATI and consider the Coulomb effect on both the trajectory and phase of the tunneled electrons.

We have seen the importance of the Coulomb potential in the formation of ATI. In the Feynman's path integral picture, the trajectories can contribute to the destructive or constructive interference that depends on the classical action along their paths. Now we investigate the classical origin of ATI patterns by tracing back the initial coordinates (tunneling phase and tunneling momentum) of electrons at the tunnel exit.

Classically, there are two kinds of tunneled electrons, i.e., direct electrons and rescattered electrons. In the Simpleman model, the electron ionized before the peak of the electric field within half an optical cycle will be pulled away from the ion directly. The electron released after the peak of the electric field will be driven back to the parent ion. Direct electrons experience a small Coulomb attraction immediately after the tunnel exit, while the rescattered electrons will be further influenced by the parent ion's potential upon their subsequent returns. In order to find the signatures of the Coulomb effect on electron trajectories and quantum interference, we trace back the initial coordinates of all of the tunneled electrons in a half laser cycle that contribute to the final PAD with different models.

Without consideration of the Coulomb effect on the trajectory and phase, all of the tunneled electrons will contribute to the final PAD, as seen in Fig. 3(a), where the initial coordinates of tunneled electrons in a half laser cycle are predicted by the ADK theory. Including the Coulomb effect, not all of tunneled electrons will contribute to the final PAD, as seen in Fig. 3(b). Compared with Fig. 3(a), the Coulomb potential has three important effects on the final PAD without considering the interference: (i) a fraction of the tunneled electrons can be recaptured by the ionic potential during electron recollision; (ii) some tunneled electrons are scattered into high energy. The initial transverse momentum distribution and the Coulomb effect

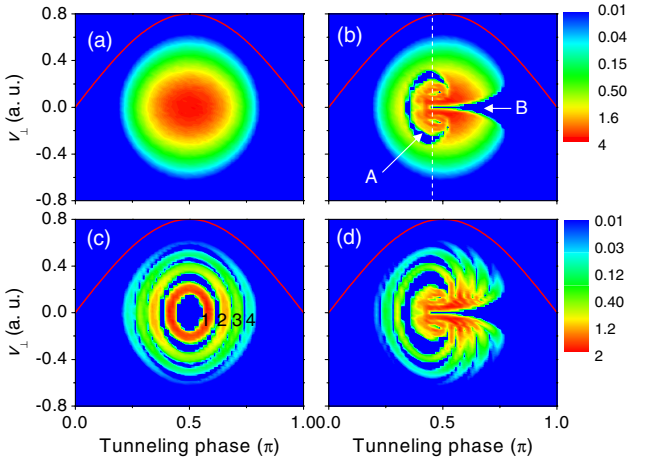

FIG. 3 (color online). The initial phase space of tunneling electrons, i.e., the tunneling probability of the initial transverse momentum with respect to the tunneling phase from a half laser cycle that contribute to the final PAD. (a) Without the Coulomb potential in the Newtonian equation and without solving the phase equation (Simplemam model), (b) with consideration of the Coulomb potential in the Newtonian equation and without solving the phase equation (CTMC model), (c) without consideration of the Coulomb potential in both the Newtonian and phase equation in the QTMC model, and (d) with consideration of the Coulomb effect in both the Newtonian and phase equation in the QTMC model.

manifest their importance in both the recapture and backscattering process. As shown in Fig. 3(b), the missing area *A* is due to the trapping of tunneled electrons by the parent ions and those electrons can be stabilized in the Rydberg states [23,24]. The missing electrons in the area *B* will contribute to high energy electrons in the plateau because of strong backward scattering [25]; and (iii) the time boundary of direct electrons and rescattered electrons is shifted ahead of the field maximum due to the Coulomb effect, indicated by the white dashed line in Fig. 3(b) [26].

If the intercycle interference is considered, depending on the initial tunneling coordinates, the tunneled electrons will contribute to the constructive or destructive interference. With the back analysis of PADs, we can identify the initial tunneling coordinates of all of the tunneled electrons. If the Coulomb effect is not considered, the initial momentum distributions that contribute to the final ATI also reveal rings, as shown in Fig. 3(c) (the corresponding ATI orders are also marked). When the effects of the Coulomb potential and interference are fully considered in the QTMC model, the initial momentum distributions of tunneled electrons that contribute to the final PADs are strongly distorted [Fig. 3(d)]. The back analysis of initial tunneling coordinates of tunneled electrons with consideration of the long-range Coulomb potential provides more sophisticated information.

In fact, both intracycle and intercycle interference will come into effect [27]. Each order ATI is composed of

several spots, e.g., the destructive or constructive interference patterns within each order of ATI. The dominant angular momentum of the first ATI ring is determined by both the Coulomb-corrected trajectory and Coulomb-corrected action. Employing the advantage of the QTMC model, we can further trace back the classical origin of each ATI spot. As shown in Figs. 4(a)–4(c), the initial transverse momentum and the tunneling phase for the tunneled electrons for three spots with positive p_z and p_r of the first-order ATI [$P_1 - P_3$ in Fig. 1(d)] are shown. Obviously, there are two types of intracycle interference to form those spots; (i) the interference between rescattered electrons (marked with R_1 and R_2) in the same field direction, where R_1 and R_2 represent the groups of tunneled electrons with large positive and small negative initial transverse momentum distributions, respectively; and (ii) the interference of direct electrons (D_1) with the rescattered electrons (R_1 or R_2). If the Coulomb effect is not considered, only the groups of R_1 and D_1 with the positive transverse momentum contribute to the final interference patterns. In the presence of the Coulomb field, another group of rescattered electrons with small negative transverse momenta (R_2) will significantly contribute to the ATI because of its higher ionization rate. The final momenta of the groups R_1, R_2, and D_1 of tunneled electrons are very similar and will show the constructive or destructive interference patterns within the ATI rings [18]. Indeed, all of the intercycle and intracycle interference of direct electrons and rescattered electrons from a long laser pulse contributes to the final PADs. The higher order ATI is mainly contributed from the interference among the rescattered electrons.

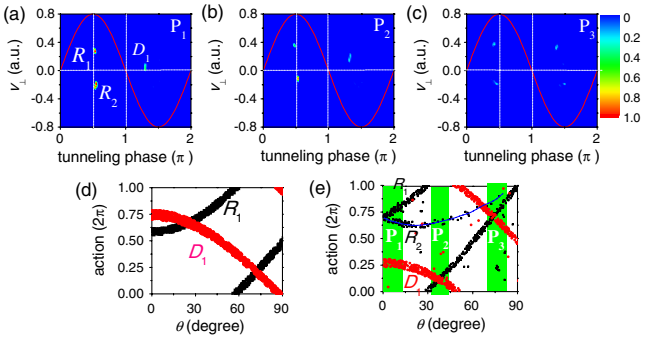

FIG. 4 (color online). (a)–(c) show the initial transverse momentum with respect to the tunneling phase of P_1, P_2, and P_3 of the first-order ATI in a laser cycle, respectively. The red solid lines show the laser field. $P_1 - P_3$ represent the three ATI spots in the first quadrant ($p_z > 0$ and $p_r > 0$) of Fig. 1(d). In (a), R_1 and R_2 indicate the group of the rescattered electrons with a larger and smaller transverse momentum, respectively. D_1 indicates the direct electrons. (d)–(e) show the electron action with respect to the emission angle $\theta = \cos^{-1}(p_z/\sqrt{p_z^2 + p_r^2})$ without the Coulomb potential (d) and with the Coulomb potential (e) for the first order ATI peaks in the quadrant I. Black (red) dots show the electrons released at the first (second) half cycle of the laser fields in (a)–(c). The trajectory weights are not included in (d) and (e). In (d), there are only the groups of R_1 and D_1. In (e), the blue solid line indicates the group of R_2 electrons. The green regions correspond to the three ATI spots of $P_1 - P_3$. The action values are normalized into an interval of $[0, 2\pi]$. The simulation parameters are the same as in Fig. 1(d).

To reveal how the intracycle interferences take place, we plot the action of tunneled electrons from the positive field and negative field in a laser cycle with respect to the emission angle in the range of 0°–90° for the first order ATI in Figs. 4(d) and 4(e) (see [18] for more details). The action difference ΔS of those groups of electrons can reflect the constructive or destructive interference of the tunneled electrons. Without including the Coulomb effect in both the electron trajectory and phase, the normalized action of two groups of electrons intersects near the angle of 0° and 75° (where ΔS is $2n\pi$, $n = 0, 1, 2, \ldots$), i.e., ATI spots are formed by the constructive interference between the R_1 and D_1 group of electrons [Fig. 4(d)]. Figure 4(f) illustrates the results with the inclusion of both the Coulomb-corrected trajectory and the Coulomb-corrected phase in the range of 0°–90° for the first-order ATI. One can find that the spot P_1 is dominantly formed by the constructive interference between R_1 and R_2, P_2 is mainly formed by R_1 and D_1, and P_3 contains contributions from all of them. Because the group of electrons of R_2 has smaller initial transverse momenta, the Coulomb potential has much stronger influence on R_2 than R_1 and D_1. The Coulomb-corrected phase will evidently slow down the increase of the action of R_2 with respect to the emission angle. Accordingly, the interference between R_1 and R_2 can give rise to more destructive patterns within an ATI ring than that in the case of neglecting the Coulomb-corrected phase [Fig. 2(d)], in which the action difference between R_1 and R_2 is nearly independent on the emission angle. The relative contribution of those trajectories will change when varying the laser intensity.

In summary, by encoding the path integral into the ADK theory, we have developed an intuitive QTMC model and have applied the model to explain the high-resolution PADs of ATI. We show that the ionic potential has a significant role on the PADs of ATI. The initial tunneling coordinates of the PADs of ATI can be resolved by the QTMC model. This model has established the classical correspondence of the quantum dynamics. The underlying electron dynamics of ATI patterns on a subcycle time scale can be described using the QTMC model, which will enable the photoelectron spectroscopy of strong-field ionization. The QTMC model provides a bridge between the tunneling theory and above-threshold ionization, and has a potential to be extended for probing molecular dynamics by combining with the MO ADK theory.

This work is supported by the 973 program (No. 2013CB922403), the NSFC (Grants No. 11125416, No. 11121091, No. 11322437, and No. 11134001). We thank Professor Reinhard Dörner for the stimulating discussions.

*qhgong@pku.edu.cn
†yunquan.liu@pku.edu.cn

[1] P. Agostini, F. Fabre, G. Mainfray, G. Petite, and N. K. Rahman, Phys. Rev. Lett. **42**, 1127 (1979).
[2] R. R. Freeman, P. H. Bucksbaum, H. Milchberg, S. Darack, D. Schumacher, and M. E. Geusic, Phys. Rev. Lett. **59**, 1092 (1987).
[3] L. V. Keldysh, Sov. Phys. JETP **20**, 1307 (1965).
[4] P. B. Corkum, Phys. Rev. Lett. **71**, 1994 (1993).
[5] W. Becker, F. Grasbon, R. Kopold, D. B. Milošević, G. G. Paulus, and H. Walther, Adv. At. Mol. Opt. Phys. **48**, 35 (2002).
[6] B. Hu, J. Liu, and S. G. Chen, Phys. Lett. A **236**, 533 (1997).
[7] T. M. Yan, S. V. Popruzhenko, M. J. J. Vrakking, and D. Bauer, Phys. Rev. Lett. **105**, 253002 (2010); T. Yan and D. Bauer, Phys. Rev. A **86**, 053403 (2012).
[8] Y. Huismans *et al.*, Science **331**, 61 (2011).
[9] T. Morishita, Z. Chen, S. Watanabe, and C. D. Lin, Phys. Rev. A **75**, 023407 (2007).
[10] M. V. Ammosov, N. B. Delone, and V. P. Krainov, Sov. Phys. JETP **64**, 1191 (1986).
[11] N. B. Delone and V. P. Krainov, J. Opt. Soc. Am. B **8**, 1207 (1991).
[12] R. P. Feynman, Rev. Mod. Phys. **20**, 367 (1948).
[13] P. A. M. Dirac, Rev. Mod. Phys. **17**, 195 (1945).
[14] P. A. M. Dirac, Phys. Z. Sowjetunion **3**, 64 (1933).
[15] P. Saliéres *et al.*, Science **292**, 902 (2001).
[16] J. Ullrich, R. Moshammer, A. Dorn, R. Dörner, L. Ph. H. Schmidt, and H. Schmidt-Böcking, Rep. Prog. Phys. **66**, 1463 (2003).
[17] L. D. Landau and E. M. Lifschitz, *Quantum Mechanics (Non-relativistic Theory)* (Oxford Univ. Press, New York, 1958).
[18] See Supplemental Material at http://link.aps.org/supplemental/10.1103/PhysRevLett.112.113002 for details.
[19] V. Schyja, T. Lang, and H. Helm, Phys. Rev. A **57**, 3692 (1998); M. Li, Y. Liu, H. Liu, Y. Yang, J. Yuan, X. Liu, Y. Deng, C. Wu, and Q. Gong, Phys. Rev. A **85**, 013414 (2012).
[20] M. J. Nandor, M. A. Walker, L. D. VanWoerkom, and H. G. Muller, Phys. Rev. A **60**, R1771 (1999).
[21] Ph. A. Korneev *et al.*, Phys. Rev. Lett. **108**, 223601 (2012).
[22] T. Brabec, M. Yu. Ivanov, and P. B. Corkum, Phys. Rev. A **54**, R2551 (1996).
[23] T. Nubbemeyer, K. Gorling, A. Saenz, U. Eichmann, and W. Sandner, Phys. Rev. Lett. **101**, 233001 (2008).
[24] H. Liu *et al.*, Phys. Rev. Lett. **109**, 093001 (2012).
[25] J. Yuan, M. Li, X. Sun, Q. Gong, and Y. Liu, J. Phys. B **47**, 015003 (2014).
[26] M. Li, Y. Liu, H. Liu, Q. Ning, L. Fu, J. Liu, Y. Deng, C. Wu, L. Peng, and Q. Gong, Phys. Rev. Lett. **111**, 023006 (2013).
[27] D. G. Arbó, K. L. Ishikawa, K. Schiessl, E. Persson, and J. Burgdorfer, Phys. Rev. A **81**, 021403(R) (2010).